Microstructural Investigation into Premature Failure of Compressor Turbine (CT) Blade Material of High Pressure (HP) PT6A-114A Engine

J. Ngoret[1,2] and V. Kommula[1]

* *jngoret@jkuat.ac.ke*

Received: February 2018 **Revised: April 2018** **Accepted: October 2018**

[1] Department of Mechanical Engineering, University of Botswana, Gaborone.

[2] Department of Mechanical Engineering, Jomo Kenyatta University of Agriculture and Technology, Nairobi, Kenya.

DOI: 10.22068/ijmse.16.1.49

Abstract: *This paper investigates premature failure of High Pressure (HP) PT6A-114A Compressor Turbine (CT) blades used for short-haul aircraft fleet at 6378 h, contrary to 10000 h pre-set by the manufacturer. The CT blades were sectioned both transversely and longitudinally and subjected to several microstructural examinations; X-ray Diffraction (XRD), X-ray Fluorescence (XRF), Energy Dispersive Spectroscopy-Scanning Electron Microscopy (EDS-SEM) of the tips, airfoils, as well as the bases. It was observed that from repeated elevated heating, incomplete dissolving and recrystallization of the substrate material, brittle carbides were initiated and developed. The tips were more affected, followed by the airfoils and least at the bases. Impingement of heat from the combustors on the CT blades led to rapid graining and rafting with eventual cracking upon cooling. The results further suggested that pores which are typically processing defects were pronounced at the bases than either at the airfoils and the tips. However, contrary to the expectation that the bases would degrade more and rapider, a more near uniform distribution of the cuboidal phase was evident relative to the tips and airfoils, confirming that degradation of the CT blades originated from creep and fatigue.*

Keywords: *Inconel 713LC, XRD, XRF, EDS - SEM*

1. INTRODUCTION

Polycrystalline Inconel 713LC, a nickel base super alloy is used for manufacture of compressor turbine (CT) blades of short-haul aircraft, the PT6A-114A engines. Its high creep-fatigue strength, toughness, ability to form stable alloys without phase instability, little or no attack from atmospheric elements, high corrosion and oxidation resistance at elevated temperatures make it ideal for the task.

However, repetitive exposure of CT blades, to severe thermo-mechanical stresses coupled with contaminants in fuel and air results in either internal and external damage of the blade material [1, 2]. Internal damage manifests as phase aging (rafting), grain growth, grain boundary creep [3], voiding, carbide precipitation and formation of brittle phases [4]. External deterioration occurs as corrosion, oxidation, micro-crack formation, erosion or fretting [5]. Both internal and external damages lead to loss of substrate materials and coatings strength [6]. Protection of the substrate material from damage is crucial enhance the health of the CT blades to avert sudden and catastrophic failures. Aluminide diffusion coating is used on Inconel 713LC CT blades [7]. The coating prolongs the life of the CT blades and guarantees reliability while in service [8]. Monitoring the microstructural changes of the substrate material and coating side by side ensures proper health status of CT blades can be accounted for [9]. As such, damage evolution, real time status and remaining useful life can then be informed [10]. This paper investigates the microstructural change within the substrate material that occasioned early retire.

2. Characteristics of the Studied Material

The elemental composition of the CT blade material in study is as presented in Table 1 [11]. Manufacture of the CT blades was done by conventional solid investment casting, while application of the aluminide coating was performed through diffusion by chemical vapor deposition (CVD).

[DOI: 10.22068/ijmse.16.1.49]

Table 1. Elements of blade material by % mass [11]

Ni	Al	Cr	Ti	Mo	C	B	P	S	Nb	Zr	Rest
74	6.1	12.5	0.8	4.2	0.05	0.012	0.006	0.004	2.1	0.1	.Bal

The various elements that constitute the material play the following important functional roles discussed below.

2. 1. Solid Solution Strengtheners

The primary aim of these elements is to increase resistance against dislocations. As the temperature rises, these elements diffuse less in Nickel as such they enhance creep resistance [12]. In Inconel 713LC, molybdenum is well known to improve resistance against non-oxidizing acids, pitting and crevice corrosions, while imparting strength to the alloy at high temperatures. Chromium on the other hand enhances the materials strength while inhibiting oxidation and sulphidation by easily precipitating into intergranular carbides. Cobalt scales down carburization and sulphidation while increasing solubility of carbon in nickel making sulphides of cobalt have higher melting point than those of nickel [13].

2.2. Precipitate Formers

Niobium in small quantities is a key grain boundary strengthener in the solvus phase as it increases yield strength and material density [13, 14]. Its presence however, accelerates the rate of fatigue crack growth [15]. Aluminum is well-known for resistance to oxidation [16], oxide spalling, carburization, chlorine attack, increases the volume and adherence of the alloys phase at high temperatures [12]. However, too much of the solvus phase weakens the material during operations.

2.3. Carbide Formers

Other than improving corrosion and creep resistance at elevated temperatures, carbides prevent grain-boundary sliding and migration. Nevertheless, they compromise materials ductility and make it susceptible to cracking [17] as such, they ought to be checked to minimize the alloys brittleness. Chromium, niobium and titanium play this important role in Inconel 713LC. Being a high content chromium alloy, readily forms from the reaction at the grain boundaries [18-20] limiting titanium to combine with carbon which is good to counter against intergranular corrosion arising from the carbides of chromium and to promote age hardening.

2.4. Phase Stabilizers and Protective Coating

Phase stabilizers are classified as external or internal. External stabilizers transforms the alloys temperature to prevent oxidation [21] in the presence of oxygen, sulphur, sodium, vanadium or other contaminants that may occasion hot corrosion [22]. Addition of chromium into the alloy leads to oxide formation which inhibits both oxidation and hot corrosion [12] since cobalt alone cannot adequately play this role owing to ready diffusivity of sulphur in it at elevated temperatures than in Ni [12, 23]. At temperatures of about 1223K Aluminium exhibits better oxidation resistance compared to chromium as tends to turn gaseous [21]. Internal stabilizers are primarily whose key function is to check sliding and migration of grain boundaries of the alloy at elevated temperature. In Inconel 713LC, Boron segregates to the grain boundaries [24] slowing down formation of carbides which improves the alloys ductility and rupture life at high temperatures. Inclusion of niobium appreciably decreases the amount of formation in the alloy [25, 26]. Following continual depletion of chromium in the alloy, undesirable grain boundary carbides associated with precipitate free zones from increased solubility of precipitates occur, leading to fall of the alloys strength. Boron is therefore included to deter this occurrence. Inclusion of zirconium in minor quantities serves to counter potential weakening of the material from presence of sulphur in fuels and operational environment. Presence of refractory elements like molybdenum assists in countering acid attacks. However, molybdenum accelerates formation of carbides from the reaction [27].

The protective aluminide coating plays a

[DOI: 10.22068/ijmse.16.1.49]

vital role in guarding the material from high temperature oxidation, hot corrosion, attack by chemical constituents in the fuel and the operational environment [11]. The diffusive aluminides coating in Inconel 713LC functions by either inward diffusion; characterized by high activity of aluminium diffusing inwards faster than nickel outwards between the Ni-Al intermetalics or outward diffusion; faster outward nickel than inward aluminium at much higher temperatures [28, 29]. Chromium and molybdenum also influence the microstructure and composition the coating, in their absence of which interdiffusion zone start to develop [30].

3. EXPERIMENTAL METHODS

3.1. Sample Preparations

In conformity to ASTM E3-11; sectioning, mounting, grinding, polishing and carbon coating were carried out. The transverse markings and sectioning were carried out at intervals of 33.3%,66.7% and 83.3% from the root of the CT blades whose lengths are 36mm to give a fair representation of the base, airfoil and tip sections as presented in Fig. 1: (a), (b), (c) and (d) while the longitudinal section marking and sectioning was midway through the blade in Fig. 2: (a) and (b).

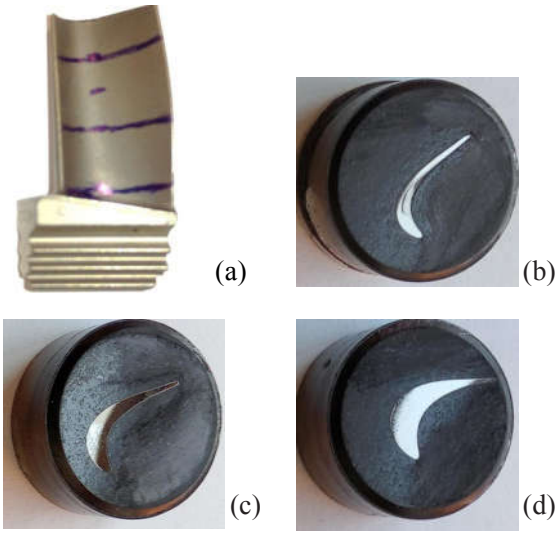

Fig. 1. (a) Marked transverse section (b) Tip (c) Airfoil (d) Base

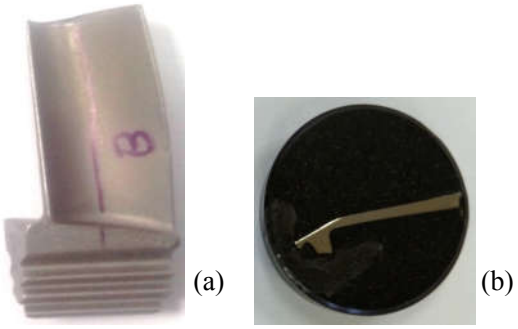

Fig. 2. (a) Marked longitudinal section (b) Sectioned

3.2. X-ray Fluorescence (XRF)

S8 Tiger, Bruker AXS, machine was used for data acquisition from the selected samples. The specimens were cleaned and placed in 25mm plastic cup sample holder and covered with Prolene seal at Standard Temperature and Pressure (STP). With the system having been calibrated by STG2 standards, the Quant-express method was used for taking readings, QE-Check-He25mm. Spectra Plus, Version 3.0.2.19 © 2012, Bruker AXS GmbH software was used for peak identification, element detection and quantification normalization.

3.3. X-Ray Diffraction (XRD)

Empyrean XRD PANalytical machine, Expert Pro. was used for data collection. The specimens were cleaned, placed on a zero-background holder and pressed to make a 5mm radius circle at STP. Scan Axis Gonio settings set prior to spinning with radiation from start position 33.64 [°2θ] to end position 93.08 [°2θ] with step sizes of 0.02 [°2θ] and scan step time of 1.00 [s]. X'Pert High Score Plus, V4.5 software was used for analysis.

3.4 Energy Dispersive Spectroscopy-Scanning Electron Microscopy (EDS-SEM)

ZEISS SEM, Gemini 500, equipped with an EDS system, AMETEK, EDAX was used for data acquisition.

[DOI: 10.22068/ijmse.16.1.49]

4. RESULTS AND DISCUSSIONS

4.1. X-Ray Fluorescence (XRF)

XRF analysis was a confirmatory test to ascertain presence of the various elements which constitute the bulk of both the coating and material of the CT blades as summarized in Table 2. The key constituent elements were positively identified are in conformity with the manufacturer's standards (Al, Cr, Mo, Ni and Ti). A number of micro trace constituent elements such as B, C, Nb and Zr were however undetected. Intruder elements were also identified possibly occurring from fuels or flight environments. They include Co, Fe and Si as shown in Table 2 as compared to those of the original material in Table 1.

The dynamics of decrease and increase of the constituent elements could be attributed to the scanned surface in comparison to the relative exposure to heat and activity of inward or outward diffusion.

4.2. X-Ray Diffraction (XRD)

XRD analysis was used for both qualitative as well as quantitative analyses. In qualitative analysis, the peak positions in a powder pattern, a representation of a phase was determined by the size, shape, and symmetry of the unit cell while the peak intensities are determined by the arrangement of atoms within that cell. In case of a phase mixture, diffraction patterns overlap making it possible to identify the components of a mixture. Using search and matching methods from powder diffraction files and contemporary algorithms, compound giving rise to the specific pattern were singled out. In quantitative analysis, for every variation of concentration phase mixture that occurred, peaks in the phase consequently varied. By measuring the intensities of peaks, concentration could then be determined. Fig. 3 reports on the XRD spectrum on which seven peaks and their relative positions were identified and are recorded in Table 3.

Table 2. XRF % elemental detection by mass

Element	Ni	Al	Co	Si	Cr	Ti	Mo	Fe
Concentration %	49.93	23.3	9.73	6.15	4.91	2.59	2.26	0.37

Table 3. XRD identified peaks, their positions and respective counts

Peak Number	1	2	3	4	5	6	7
Position [°2θ]	35.64	36.29	43.94	50.75	63.32	74.98	91.08
Height (Counts)	392.04	392.04	15725.16	2693.61	129.96	2981.16	2043.04

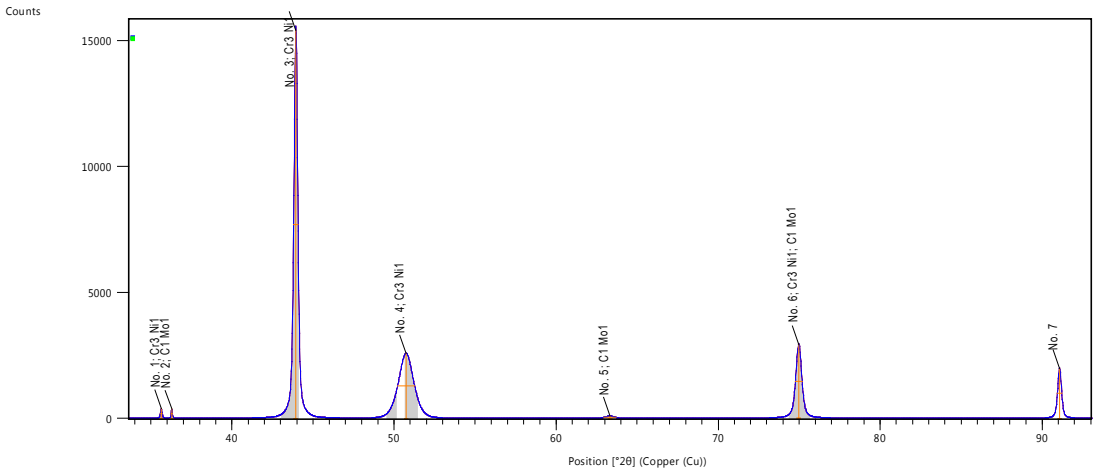

Fig. 3. XRD analysis

[DOI: 10.22068/ijmse.16.1.49]

Two compounds predominantly formed the bulk of the peaks; and . The constituent elements of these compounds form the bulk of the base and alloying materials in Inconel 713LC.

One other peak number 7 in the XRD pattern could not match any PAN ICSD Database FIZ Karlsruhe 2016-1 for High Score (Plus) V3. X. In this case it was omitted in the analyses. This could have been occasioned by the scanned surfaces of the samples being smaller than 5mm holder space, resulting in low intensity peaks which were also very close to the background noise making it difficult to be tapped despite scanning having lasted for over one hour of scan time per sample.

4.3. SEM-EDS Analyses

4.3.1. The Tip

The tip section had cracks originating from the protective coating and finding their way to the substrate material. Pores were evident and needles had developed as they appear in Fig. 4.

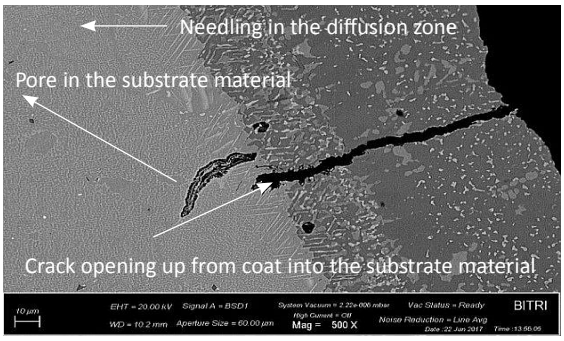

Fig. 4. Sectioned tip

Selected areas 4, 5 and 6 as shown in Fig. 5 were chosen for EDS analyses.

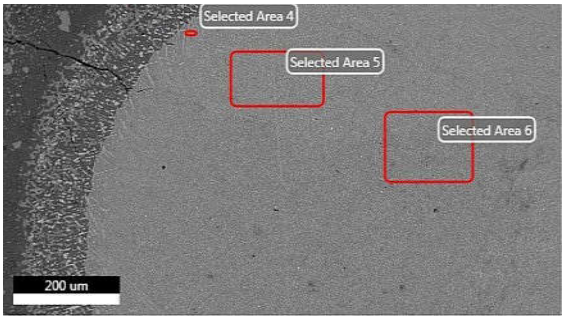

Fig. 5. EDS micrograph of sectioned tip

The EDS spectra of selected areas 4, in Fig. 6 had a great inward diffusion of Al than outward diffusion of Ni. It also equally had traces oxides of Si, Fe, and Cu, possibly from the fuel constituents and flight environment. Carbides of Mo, Ti, V, Cr and Co were present.

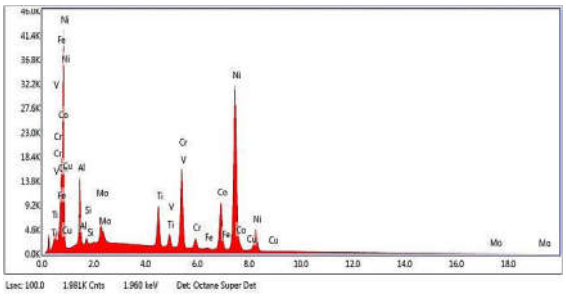

Fig. 6. EDS spectrum of selected area 4

Spectra for selected areas 5 and 6 in Figs. 7 and 8 had more or less similar characteristics; decreased Al inward diffusion and increased outward Ni diffusion. No traces of oxides from Si, Fe and Cu were found. The two areas equally exhibited a drop-in carbide of Mo and Cr, relative to selected area 4, but an increase in carbides of Co. V decreased in selected area 5 compared to 4 and was absolutely nonexistent in selected area 6.

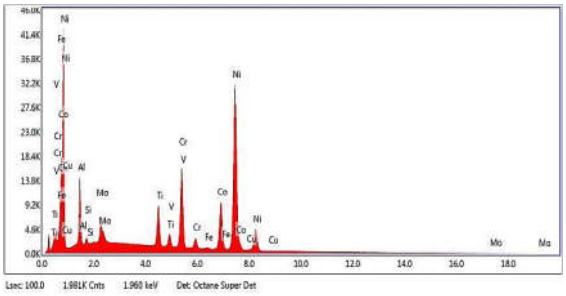

Fig. 7. EDS spectrum of selected area 5

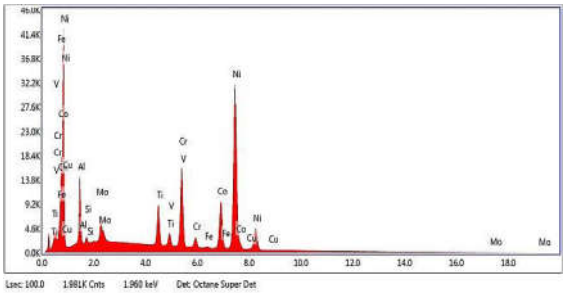

Fig. 8. EDS spectrum of selected area 6

Table 4 records the EDS elemental composition of the tip at selected areas 4 – 6 in Figs. 6-8.

[DOI: 10.22068/ijmse.16.1.49]

Table 4. Elemental composition of the tip at selected areas 4-6

Element	AlK	SiK	MoL	TiK	VK	CrK	FeK	CoK	NiK	CuK
Weight Selected Area 4 %	6.4	0.4	3.0	4.6	1.2	12.3	0.4	13.8	57.8	0.3
Weight Selected Area 5 %	5.4	0.0	2.2	4.4	0.9	9.3	0.3	14.5	62.9	-
Weight Selected Area 6 %	5.6	0.0	2.2	4.7	-	9.1	0.3	14.2	63.8	-

For the tips which are the hottest regions of the CT blade indicated considerable magnitude of deterioration of microstructure. Primary original metal carbides near evenly perfect cuboidal phase of had degenerated and transformed into , and . As a result, rafting and elongation of the later carbides led weakening the material structure and upon cooling, cracking was ultimately inevitable. Such attacks were prominent at the leading edges of the blades than the trailing edges, airfoils, and base regions as confirmed by the temperature modeling results.

4.3.2. The Airfoil

The micrograph in Fig. 9 presents evidence of pores with dispersions of white Ti carbides.

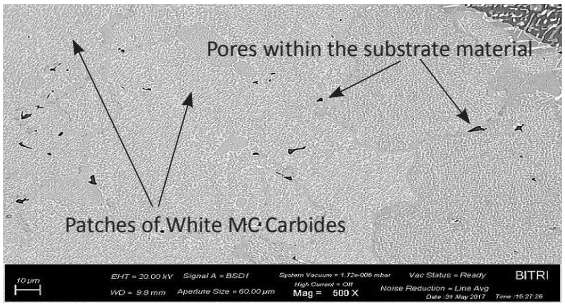

Fig. 9. Sectioned airfoil (Image 1)

Grains had also developed gray carbides, as depicted in Fig. 10 arising from decomposing of carbides after repetitive exposure to elevated temperatures. As a result, rafting is evident but, a much lower level compared to the tip.

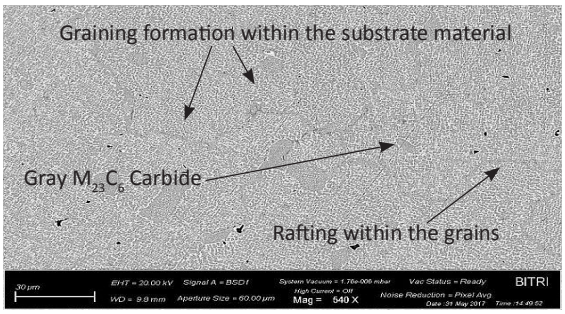

Fig. 10. Sectioned airfoil (Image 2)

The EDS spectra of the airfoil in Figs. 11, 12, 13 and 14 indicate uniform degradation of the material compared to the tip. For the same selected areas, carbides of Mo, Ti, Cr and Co were averagely similar too, with traces of Fe also detected in relatively equal measures. Inward Al diffusion besides outward Ni diffusion concurrently occurred.

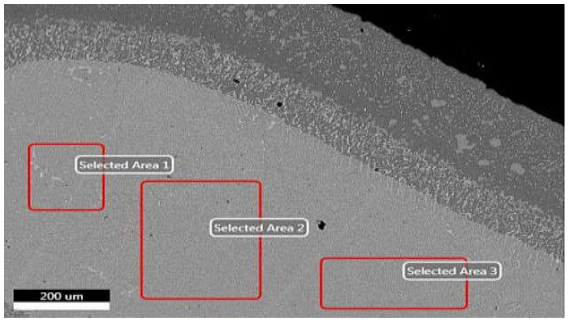

Fig. 11. EDS micrograph of sectioned airfoil

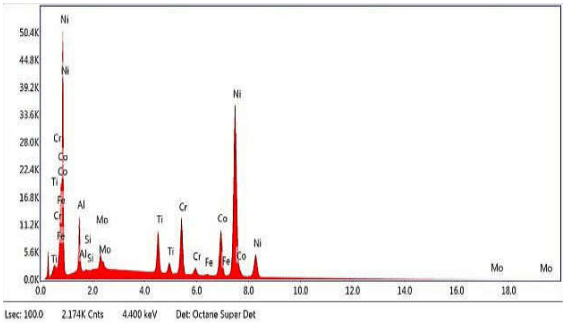

Fig. 12. EDS spectrum of selected area 1

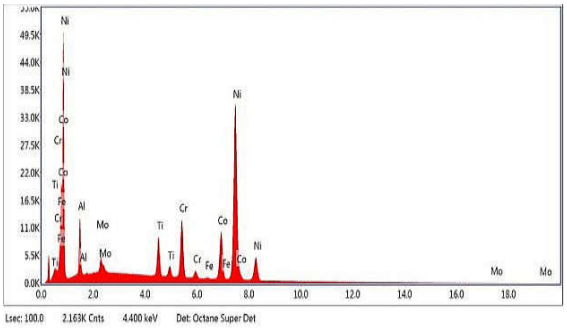

Fig. 13. EDS spectrum of selected area 2

[DOI: 10.22068/ijmse.16.1.49]

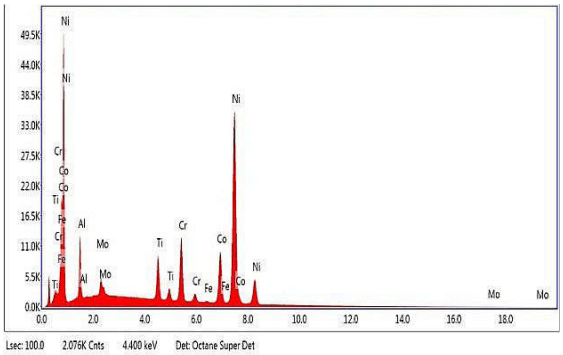

Fig. 14. EDS spectrum of selected area 3

Table 5 indicates the elemental composition of the airfoil at selected areas 1-3 in Figs. 12-14.

The inner material within the depletion zone of the airfoil in Fig. 15 experienced pronounced rafting.

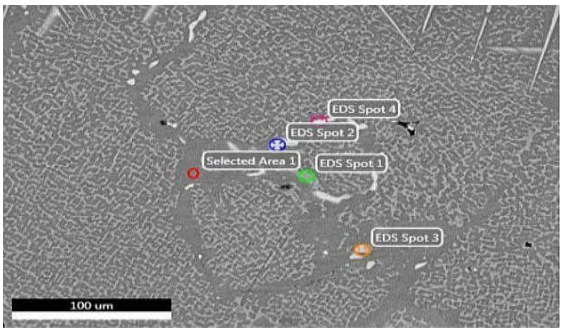

Fig. 15. Sectioned airfoil inner material within the depletion zone

Selected area 1, in Fig. 16 confirmed both active Al inward and outward Ni diffusions. Carbides of Mo, Cr, Co dropped, while Ti carbides significantly increased. Occurrence of V was also occasioned.

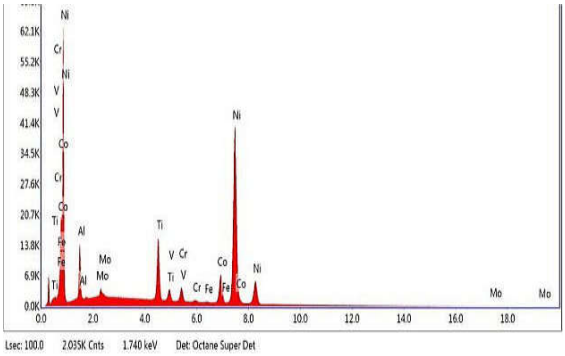

Fig. 16. EDS spectrum of selected area 1

EDS spots 1 in Fig. 17 depicted a significant increase in carbides of Cr and Co. Carbides of Mo and V had slightly increased while Ti carbides had dropped. Traces of Si were identified with inactivity of both inward Al and outward Ni diffusion recorded.

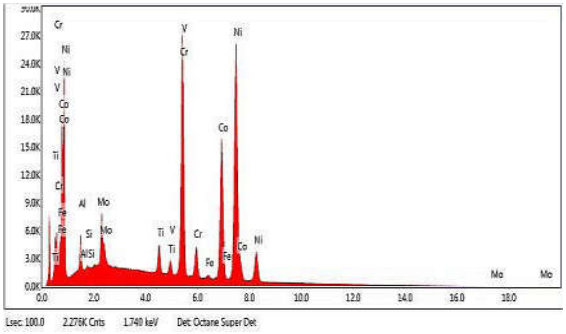

Fig. 17. EDS spectrum of spot 1

EDS spot 2 adjacent to carbides of Mo and Cr in Fig. 18 indicated slight increase in carbides of Ti. Co carbides dropped while V completely disappeared. Significant fall in activity of both inward Al and outward Ni diffusion was noted as Si and Fe presence remained unaltered.

Table 5. Elemental composition of airfoil at selected areas 1-3

Element	AlK	MoL	TiK	CrK	FeK	CoK	NiK
Weight Selected Area 1 %	5.6	2.9	5.4	9.1	0.2	13.5	63.2
Weight Selected Area 2 %	5.7	2.8	5.0	9.1	0.1	13.7	63.6
Weight Selected Area 3 %	5.6	2.8	5.1	9.3	0.3	13.7	63.1

[DOI: 10.22068/ijmse.16.1.49]

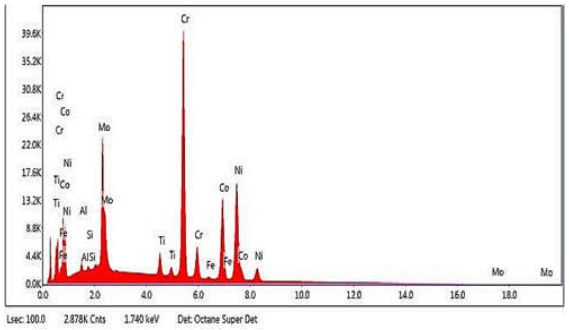

Fig. 18. EDS spectrum of spot 2

EDS spot 3 in Fig. 19 affirmed occurrence of white carbides of Cr with a slight drop of diffusion activity for both Al and Ni. Si had also significantly risen.

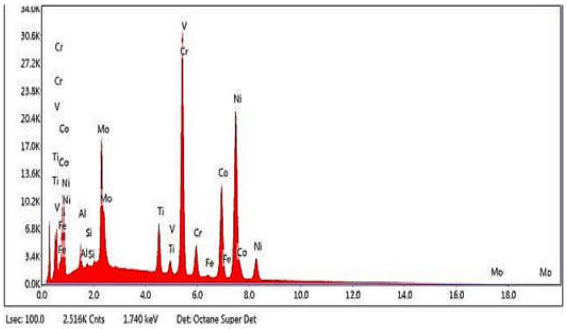

Fig. 19. EDS spectrum of spot 3

EDS spot 4 in Fig. 20 recorded an increase in carbides of Mo, Ti and Cr, while carbides of Co dropped. There was a fall in V and Fe. Relative to EDS spot 2, Al activity had slightly increased, while Ni activity significantly dropped.

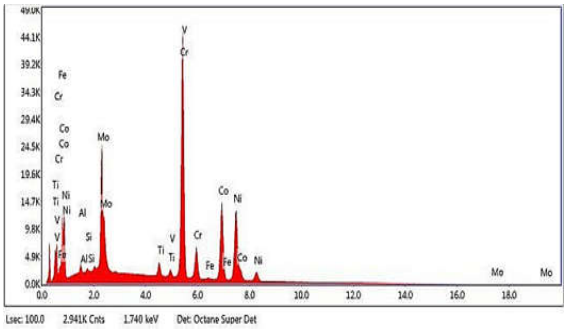

Fig. 20. EDS spectrum of spot 4

Table 6 denotes the EDS elemental composition of the airfoil's inner material within the depletion zone for selected area 1 and EDS spots 1-4, in Figs. 16-20.

4.3.3 The Base

Pores which are manufacturing defects could be identified at the base as shown in Fig. 21. However, contrary to presence of pores being thought to create potential weak points within the material, the base seemingly had a nearer uniform distribution of cuboidal phase as likened to the tip and airfoil. eutectic carbides were also noticed occasioned by slow heating up in this region, resulting in much longer heat retention, as such upon cooling, gradual precipitation is inevitable. Dispersions of white carbides of Cr at the grain boundaries were evident from incomplete solutioning of the material as it ages.

Table 6. Elemental composition of airfoil at selected areas 1-4; the depletion zone

Element	AlK	SiK	MoL	TiK	VK	CrK	FeK	CoK	NiK
Weight Selected Area 1 %	6.2	-	1.5	9.0	0.6	2.4	0.2	9.1	70.9
Weight EDS Spot 1 %	1.9	0.1	4.7	1.9	0.9	21.4	0.5	22.7	45.9
Weight EDS Spot 2 %	0.6	0.1	15.8	2.3	-	33.7	0.4	19.5	27.6
Weight EDS Spot 3 %	1.5	0.6	12.3	4.0	0.7	26.1	0.3	17.4	37.5
Weight EDS Spot 4 %	0.7	0.2	16.4	1.6	0.8	37.2	0.5	20.7	22.1

[DOI: 10.22068/ijmse.16.1.49]

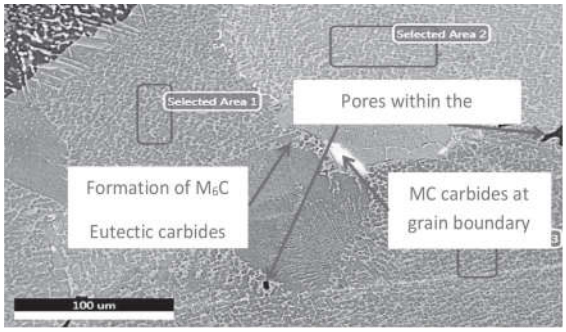

Fig. 21. Sectioned base

Carbides of Mo, V and Cr, were averagely uniformly distributed. A fairly similar inward Al as well as outward Ni diffusions was noted at the selected areas 1-3 at the base represented in Figs. 22, 23 and 24.

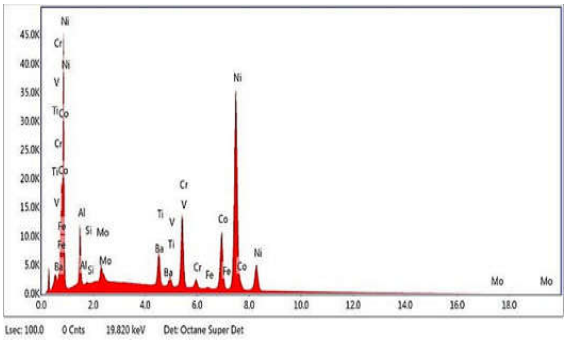

Fig. 22. EDS spectrum of selected area 1

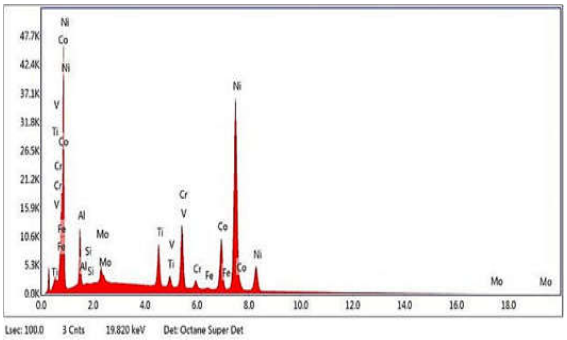

Fig. 23. EDS spectrum of selected area 2

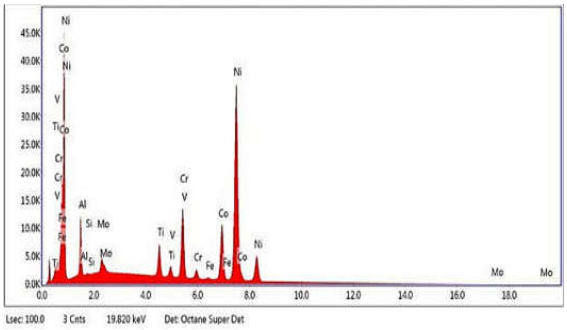

Fig. 24. EDS spectrum of selected area 3

Table 7 indicates the EDS elemental composition of the base for selected areas 1-3, in Figs. 22-24.

Further within the base in the depleted zone too, phases had formed as illustrated by the sets of selected areas pairing within the grains in Fig. 25. The elemental analysis of these areas are shown as follow: selected areas 1 and 2 in Figs. 26 and 27, selected areas 3 and 4 in Figs. 28 and 29, selected areas 5 and 6 in Figs. 30 and 31, and, selected areas 7 and 8 in Figs. 32 and 33. Their spectra however reported averagely similar quantities of material composition, an indicator of uniform aging of material in that region. Active inward Al and outward Ni diffusions were evident. No traces of oxidation were noted, with primary carbides evenly distributed throughout the region.

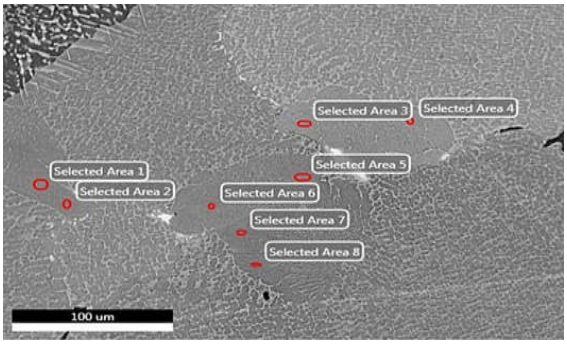

Fig. 25. Sectioned base; phases within the depleted zone in the grain

Table 7. Elemental composition of the base at selected areas 1-3

Element	AlK	MoL	TiK	VK	CrK	FeK	CoK	NiK
Weight Selected Grain Area 1 %	5.1	2.0	3.7	0.8	9.8	0.3	14.9	62.7
Weight Selected Grain Area 2 %	5.3	2.0	4.6	0.8	9.1	0.3	14.2	63.8
Weight Selected Grain Area 3 %	5.2	2.0	3.4	0.9	9.6	0.4	15.0	63.5

[DOI: 10.22068/ijmse.16.1.49]

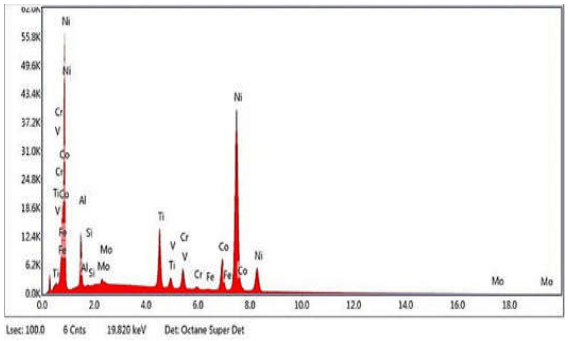

Fig. 26. EDS spectrum of selected area 1

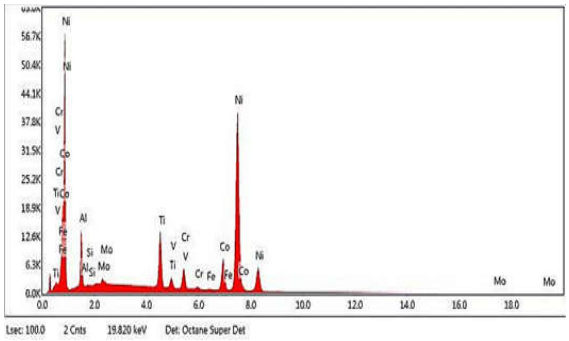

Fig. 30. EDS spectrum of selected area 5

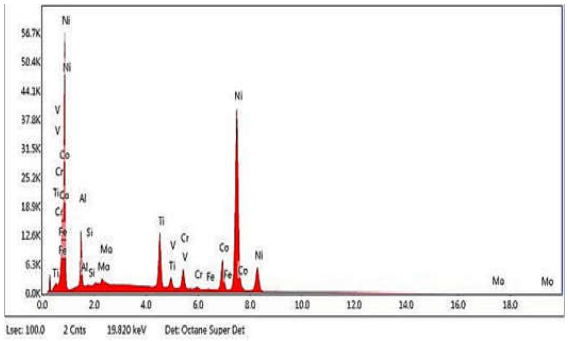

Fig. 27. EDS spectrum of selected area 2

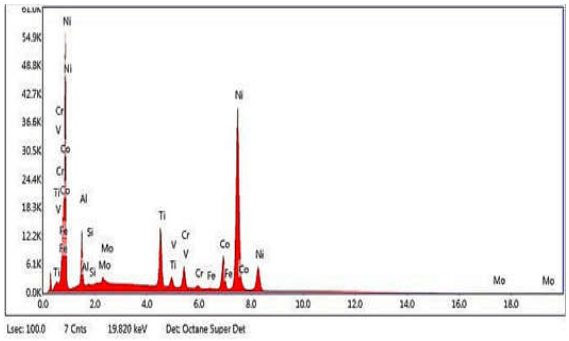

Fig. 31. EDS spectrum of selected area 6

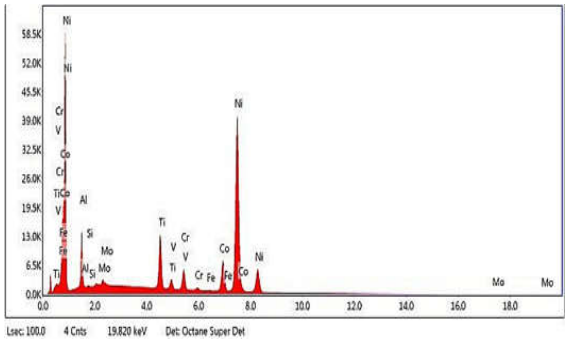

Fig. 28. EDS spectrum of selected area 3

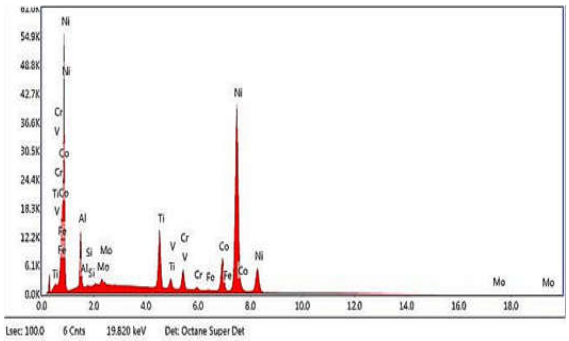

Fig. 32. EDS spectrum of selected area 7

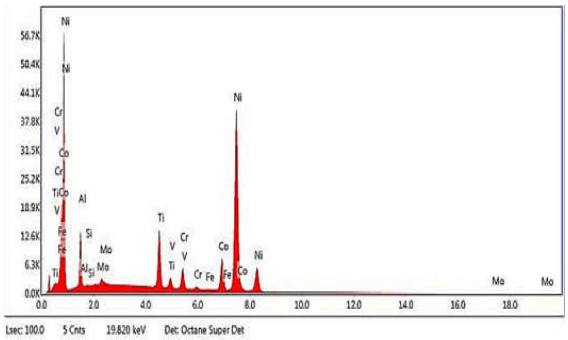

Fig. 29. EDS spectrum of selected area 4

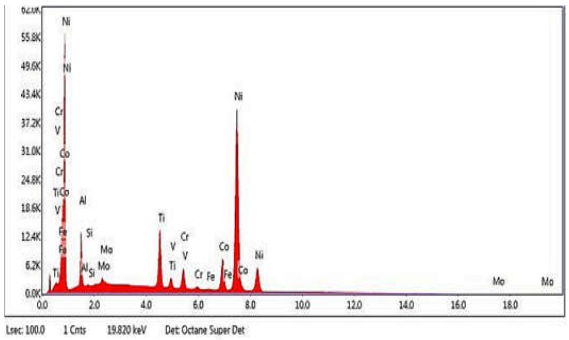

Fig. 33. EDS spectrum of selected area 8

[DOI: 10.22068/ijmse.16.1.49]

Table 8. Elemental composition of the base at selected areas 1-8

Element	AlK	MoL	TiK	VK	CrK	FeK	CoK	NiK
Weight Selected Area 1 %	6.1	0.8	7.6	0.6	3.4	0.2	10.1	71.4
Weight Selected Area 2 %	6.3	0.8	7.0	0.6	3.2	0.2	9.6	72.2
Weight Selected Area 3 %	6.5	0.9	7.0	0.6	3.5	0.2	10.1	71.3
Weight Selected Area 4 %	6.2	0.8	7.5	0.5	3.3	0.1	10.1	71.6
Weight Selected Area 5 %	6.3	0.8	7.2	0.6	3.4	0.2	10.1	71.4
Weight Selected Area 6 %	6.1	0.8	7.4	0.6	3.4	0.2	10.5	71.1
Weight Selected Area 7 %	6.1	0.8	7.2	0.6	3.2	0.2	10.3	71.6
Weight Selected Area 8 %	6.0	0.8	7.3	0.5	3.4	0.2	10.1	71.6

Table 8 depicts the EDS elemental composition of the base for selected areas 1-8, in Figs. 26–33.

5. CONCLUSION

This study performed a microstructural investigation into premature failure of compressor turbine (CT) blade material of PT6A-114A Engine. The XRF results affirmed the existence of the bulk base elements from the manufacturers' specification, while the XRD analyses enabled positive identification of the resultant compounds that constituted the substrate material after exposure to service. The EDS-SEM results established that the protective coating at the tips had been severely damaged compared to the airfoils and the bases. The pores at the bases of the CT blades were found not influence distribution of uniform cuboidal phase at the bases in comparison the rafted tips and airfoils. This confirmed that degradation of the substrate material occurred as a result of creep and fatigue and not from manufacturing defects.

6. ACKNOWLEDGEMENTS

Sincere gratitude to Office of Research and Development (ORD), University of Botswana (UB) for financing the study, Vector Aerospace Kenya Limited allowing us collect samples and data and Mobility to Enhance Training of Engineering Graduates in Africa (METEGA).

REFERENCES

1. Tamarin, Y., "Protective coatings for turbine blades", ed. A.S.M. International. Ohio, USA, 2002, 97-113.
2. Huang, Z., Wang, Z., Zhu, S., Yuan, F., and Wang, F., "Thermomechanical fatigue behavior and life prediction of a cast nickel-based superalloy". Mater. Sci. Eng., A, 2006, 432, 308-316.
3. Pollock, T. M. and Tin, S., "Nickel-based superalloys for advanced turbine engines: chemistry, microstructure and properties." J. Propul. Power, 2006, 22, 361-374.
4. Swaminathan, V., Cheruvu, N., Klein, J., and Robinson, W., "Microstructure and property assessment of conventionally cast and directionally solidified buckets refurbished after long-term service." Proceedings of the ASME 1998 International Gas Turbine and Aeroengine Congress and Exhibition, New York, USA, 1998, V005T012A013-V005T012A013.
5. Carter, T. J., "Common failures in gas turbine blades". Eng. Fail. Anal., 2005, 12, 237-247.
6. Pineau, A. and Antolovich, S. D., "High temperature fatigue of nickel-base superalloys–a review with special emphasis on deformation modes and oxidation." Eng. Fail. Anal., 2009, 16, 2668-2697.
7. Kianicová, M., "Microstructural Behaviour of Protective AlSi Coatings under Thermal Load." Adv. Mil. Technol., 2009, 4, 23-29.
8. Becker, W. T., Shipley, R. J., Lampman, S. R., Sanders, B. R., Anton, G. J., Hrivnak, N., . . . Henry, S. D., ASM handbook. Fail. Anal. Prev., 2002, 11, 1072.
9. Kargarnejad, S. and Djavanroodi, F., "Failure assessment of Nimonic 80A gas turbine blade." Eng. Fail. Anal., 2012, 26, 211-219.
10. Pahlavanyali, S., Wood, M., and Marchant, G., "Microstructural evolutions of IN738LC during multiple reheat treatment and aging." Int. Heat

[DOI: 10.22068/ijmse.16.1.49]

Treat. Surf. Eng., 2012, 6, 107-114.
11. Zielińska, M., Sieniawski, J., Yavorska, M., and Motyka, M., "Influence of chemical composition of nickel based superalloy on the formation of aluminide coatings." Arch. Metall. Mat., 2011, 56, 193-197.
12. Jena, A. and Chaturvedi, M., "The role of alloying elements in the design of nickel-base superalloys." J. Mater. Sci., 1984, 19, 3121-3139.
13. Balikci, E. and Raman, A., "Characteristics of the γ′ precipitates at high temperatures in Ni-base polycrystalline superalloy IN738LC." J. Mater. Sci., 2000, 35, 3593-3597.
14. Zhao, K., Lou, L., Ma, Y., and Hu, Z., "Effect of minor niobium addition on microstructure of a nickel-base directionally solidified superalloy." Mater. Sci. Eng., A, 2008, 476, 372-377.
15. Smith, G. and Patel, S., "The role of niobium in wrought precipitation-hardened nickel-base alloys". Superalloys 718, 625, 706 and Derivatives 2005, 718, 625-706.
16. Wallwork, G. and Hed, A., "Some limiting factors in the use of alloys at high temperatures." Oxid. Met., 1971, 3, 171-184.
17. Qin, X., Guo, J. T., Yuan, C., Hou, J. S., and Ye, H. Q., "Degeneration of primary MC carbide in a cast Ni-base superalloy." Proceedings of the Mater. Sci. Forum, 2007, 1301-1304.
18. Liu, L., Jin, T., Zhao, N., Sun, X., Guan, H., and Hu, Z., "Formation of carbides and their effects on stress rupture of a Ni-base single crystal superalloy." Mater. Sci. Eng., A, 2003, 361, 191-197.
19. Pollock, T. and Field, R., "Dislocations and high-temperature plastic deformation of superalloy single crystals." Dislocations in solids, 2002, 11, 547-618.
20. Qin, X., Guo, J., Yuan, C., Chen, C., Hou, J., and Ye, H.,"Decomposition of primary MC carbide and its effects on the fracture behaviors of a cast Ni-base superalloy." Mater. Sci. Eng., A, 2008, 485, 74-79.
21. Whittle, D. and Stringer, J., "Improvements in high temperature oxidation resistance by additions of reactive elements or oxide dispersions." Philos. Trans. R. Soc. London, Ser. A, 1980, 295, 309-329.
22. Sims, C., "The superalloys", ed. W.C. Hagel. New York, USA, 1972, 379-445.
23. Seybolt, A. and Beltran, A., "Hot Corrosion in Gas Turbines", ed. A.S.M. International. New York, USA, 1967, 251-263.
24. Yan, B., Zhang, J., and Lou, L., "Effect of boron additions on the microstructure and transverse properties of a directionally solidified superalloy." Mater. Sci. Eng., A, 2008, 474, 39-47.
25. Qin, X., Guo, J., Yuan, C., Hou, J., and Ye, H., "Thermal stability of primary carbides and carbonitrides in two cast Ni-base superalloys." Mater. Lett., 2008, 62, 2275-2278.
26. Barbosa, C., Nascimento, J., Caminha, I., and Abud, I., "Microstructural aspects of the failure analysis of nickel base superalloys components." Eng. Fail. Anal., 2005, 12, 348-361.
27. Qin, X., Guo, J., Yuan, C., Hou, J., Zhou, L., and Ye, H., "Long-term thermal exposure responses of the microstructure and properties of a cast Ni-base superalloy." Mater. Sci. Eng., A, 2012, 543, 121-128.
28. Hardwicke, C. U. and Lau, Y. C., "Advances in thermal spray coatings for gas turbines and energy generation: a review." J. Therm. Spray Technol., 2013, 22, 564-576.
29. Juliš, M., Obrtlík, K., Pospíšilová, S., Podrábský, T., and Poláka, J., "Effect of Al-Si diffusion coating on the fatigue behavior of cast Inconel 713LC at 800 C." Procedia Eng., 2010, 2, 1983-1989.
30. Davis, J. R., ASM specialty handbook: heat-resistant materials, ed. B.R. Sanders. New York, USA, 1997, 331-383.

[DOI: 10.22068/ijmse.16.1.49]